How to recover Marcus theory with fewest switches surface hopping: Add just a touch of decoherence

Brian R. Landry and Joseph E. Subotnik

Citation: J. Chem. Phys. **137**, 22A513 (2012); doi: 10.1063/1.4733675
View online: http://dx.doi.org/10.1063/1.4733675
View Table of Contents: http://jcp.aip.org/resource/1/JCPSA6/v137/i22
Published by the American Institute of Physics.

How to recover Marcus theory with fewest switches surface hopping: Add just a touch of decoherence

Brian R. Landry and Joseph E. Subotnik
Department of Chemistry, University of Pennsylvania, 231 S. 34th Street, Philadelphia, Pennsylvania 19104, USA

(Received 9 April 2012; accepted 21 June 2012; published online 31 July 2012)

We present a slightly improved version of our augmented fewest switches surface hopping (A-FSSH) algorithm and apply it to the calculation of transition rates between diabatic electronic states within the spin-boson model. We compare A-FSSH rates with (i) Marcus rates from the golden rule, (ii) Tully-style FSSH rates, and (iii) FSSH rates using a simple, intuitive decoherence criterion. We show that unlike FSSH, A-FSSH recovers the correct scaling with diabatic coupling (quadratic in V) as well as the lack of dependence on harmonic frequency ω for small enough values of ω and large enough temperatures. © *2012 American Institute of Physics*. [http://dx.doi.org/10.1063/1.4733675]

I. INTRODUCTION

Achieving efficient and accurate simulations of photochemical reaction dynamics is an important, but not fully solved problem in the field of computational chemistry. Because photochemical reactions involve electronic excitations coupled to nuclear motion, which invalidate the Born-Oppenheimer approximation, standard tools in computational chemistry are mostly inapplicable. In particular, computational chemistry today excels in two areas: (i) from the perspective of electronic structure theory, modern software packages can calculate adiabatic surfaces routinely and thus model vibrational and electronic excitation energies; (ii) from the perspective of chemical dynamics, modern biosimulation programs excel at modeling the motion of large proteins using either approximate force fields or rigorous *ab-initio* potential energy surfaces (see previous). When the Born-Oppenheimer approximation breaks down, however, multiple adiabatic electronic states become coupled and standard computational chemistry leaves its comfort zone; the two step approach described above is no longer sufficient.

Despite the difficulty inherent to nonadiabatic problems, several methods do exist in the literature for modeling electronic relaxation and nuclear friction at the same time, thus propagating both the nuclei and electrons.[1–4] Perhaps the most efficient and conceptually simple is due to Tully.[5] According to Tully, one should treat the nuclei completely classically and the electrons quantum mechanically, resulting in accelerated calculations compared with true quantum dynamics. This classical assumption is intuitively reasonable because nuclei are relatively massive whereas electrons are relatively light. In particular, according to Tully, mixed quantum-classical dynamics is modeled by three distinct processes: (i) each classical particle moves along one adiabatic surface, (ii) the electronic wavefunction associated with each classical trajectory is propagated using the electronic time-dependent Schrodinger equation with the classical nuclear positions treated as parameters, and (iii) just as the nuclear positions influence the electronic wavefunction as parameters in the time-dependent Schrodinger equation, the electronic wavefunction affects the nuclei, by playing a role in determining if the nuclear trajectory will hop from the current adiabatic surface to another surface. Surface hops maintain consistency between the projection of the electronic wavefunction onto each surface and the population of nuclear trajectories moving along that surface. Tully chose as his hopping rate the minimum rate that would enforce this consistency, and fewest switches surface hopping (FSSH) was born.

Although FSSH is used widely to model nonadiabatic processes,[5–11] the method cannot be derived and has several deficiencies as compared to exact quantum dynamics, some intentional and some unintentional.[12–17] At bottom, these deficiencies are the result of treating the nuclei classically. On the one hand, the FSSH algorithm was designed specifically to sacrifice nuclear quantum effects for computational efficiency, and thus, the intentional failures of FSSH are that the algorithm neglects tunneling and the effects of zero point energy. On the other hand, standard FSSH has other unintentional shortcomings caused by a necessarily asymmetric treatment of a quantum system interacting with a classical system. In particular and most importantly, FSSH's quantum-classical asymmetry leads to an overcoherence in the electronic wavefunction when a nuclear trajectory passes through a region of derivative coupling. More specifically, after leaving a region of derivative coupling, the electronic wavefunction has probability density on multiple surfaces corresponding to a superposition of two nuclear wave packets on different electronic surfaces. Each nuclear trajectory, however, propagates along only one surface, representing wave packet motion on a single surface in a region without derivative coupling. In this way, the electronic wavefunction is overcoherent. This mishandling of the interaction between the quantum and classical subsystems is known as the decoherence problem and can lead to spurious results even if the classical approximation itself is sound.[18–33]

In order to probe this decoherence problem in FSSH, we need a dynamical test that is sensitive to the effects of

decoherence. Recent work has shown that the decoherence problem is exposed and amplified when nuclei travel multiple times through regions of derivative coupling.[9,15–17,34,35] Thus, transition rates should provide a strong test of decoherence because over the course of a long time, one trajectory can pass through a coupling region many times before relaxing into the product well. In fact, we have shown recently that for the spin-boson model it is necessary to include decoherence to recover the correct *scaling* of Marcus transfer rates.[36] In Ref. 36 we used a simple model to add decoherence to the FSSH algorithm, and in doing so, proved that adding decoherence recovers the correct scaling. However, the simple decoherence model in Ref. 36 can be applied only (i) when the full potential energy surfaces are known and (ii) when the driving force is very different from the reorganization energy. Clearly a more general method is needed, and we believe that our augmented fewest switches surface hopping (A-FSSH) algorithm can fill that role.[16,37] In A-FSSH the decoherence mechanism works by stochastically collapsing the electronic wavefunction associated with the nuclear trajectories according to a rate that is calculated on-the-fly. The decoherence rate is based on position and momentum moments that are propagated along with the other dynamical variables (position and momentum), and we follow Tully's insight by enforcing the fewest number of collapsing events while still insisting on a necessary rate of decoherence. This more sophisticated collapse criterion leads to a general algorithm (A-FSSH) that is free from any *ad hoc* parameterization and can be applied to any molecular system of interest. In this paper, we present a slightly improved and more stable version of our A-FSSH algorithm (compared to Refs. 16 and 37), and we evaluate it with the same spin-boson system from Ref. 36 only now for a much broader and inclusive parameter regime. We show that A-FSSH reproduces the correct Marcus scaling.

This paper is structured as follows. We start by setting our notation in Sec. II. In Sec. III we review FSSH and discuss how it fails to handle electron decoherence correctly. In Sec. IV we review A-FSSH and lay out explicitly our slightly modified and improved A-FSSH method. Section V presents the details of our application of A-FSSH to the specific problem of determining transition rates for the spin-boson system. In Sec. VI we show the results of A-FSSH and compare them to FSSH. Finally, we conclude in Sec. VII with a look toward future work.

II. NOTATION

With both nuclei and electrons, as well as a mix of classical and quantum degrees of freedom, notation has the possibility of getting somewhat confusing. To be as clear as possible we use this section to discuss our usage. We write classical variables that have the potential of being multi-dimensional vectors with the vector arrow, such as the total nuclear position vector $\vec{R}$. We denote each component of classical vectors with a superscript label as in R^α. Throughout we use (i) uppercase letters for nuclear coordinates and momenta (R, P), (ii) lowercase Greek for nuclear components (α,β), and (iii) lowercase Roman for electronic components (i, j, k). There are two types of quantum mechanical operators that we consider, nuclear operators and electronic operators. Nuclear operators we write in bold as in the total nuclear position operator $\vec{\mathbf{R}}$, and we write electronic operators with a hat as in the reduced electronic density matrix $\hat{\sigma} = Tr_N \hat{\boldsymbol{\rho}}$. We do consider quantum operators that are both nuclear and electronic such as the total density operator $\hat{\boldsymbol{\rho}}$ (bold and hat). We employ the basis of adiabatic states which are parameterized by the nuclear positions for the electronic operators, and we write $|\Phi_i(\vec{R})\rangle$ for the ith state. We denote an element of a purely electronic operator in the adiabatic basis (at nuclear position $\vec{R}$) using subscripts, i.e., the reduced electronic density matrix $\langle\Phi_i(\vec{R})|\hat{\sigma}|\Phi_j(\vec{R})\rangle = \sigma_{ij}$.

III. FEWEST SWITCHES SURFACE HOPPING AND DECOHERENCE

A. Review of FSSH

Tully's fewest switches surface hopping method[5] is a mixed quantum-classical algorithm that treats the nuclei as classical particles moving along adiabatic potential energy surfaces created by the quantum mechanical electrons. The objective of FSSH is to model the classical density on each surface, and therefore the diagonal elements of a mixed quantum-classical density matrix. In order to approximate the density on each surface, FSSH employs a swarm of classical nuclear trajectories each with an associated electronic wavefunction. For the purposes of this discussion of the FSSH algorithm, we assume that we have directly computed the adiabatic potential energy surfaces, which are the eigenvalues of the electronic Hamiltonian ($\hat{V}$),

$$\hat{V}(\vec{R})|\Phi_i(\vec{R})\rangle = E_i(\vec{R})|\Phi_i(\vec{R})\rangle. \tag{1}$$

As always, the full Hamiltonian can be written as the electronic Hamiltonian plus the nuclear kinetic energy $\hat{\mathbf{H}} = \hat{\mathbf{V}} + \mathbf{T}_{nuc}$.

Once the adiabatic potential energy surfaces are known, carrying out the mixed quantum-classical dynamics involves three distinct processes. First, each nuclear trajectory moves classically along a single surface (e.g., $E_i(\vec{R})$ the ith surface), which we call the active surface. Second, we evolve the electronic statevector, $\vec{c}$, associated with each nuclear trajectory according to the Schrodinger equation with the classical nuclear positions taken as parameters:

$$\frac{dc_j}{dt} = -\frac{i}{\hbar}\sum_k V_{jk}\,c_k - \sum_{k,\alpha}\frac{P^\alpha}{M^\alpha}\,d^\alpha_{jk}\,c_k, \tag{2}$$

where $d^\alpha_{jk}(\vec{R}) = \langle\Phi_j(\vec{R})|\frac{\partial}{\partial R^\alpha}|\Phi_k(\vec{R})\rangle$ is the derivative coupling matrix and $V_{jk}(\vec{R}) = \langle\Phi_j(\vec{R})|\hat{V}(\vec{R})|\Phi_k(\vec{R})\rangle$ is the potential energy matrix. We can also consider the equivalent equation in the density matrix formulation:

$$\frac{d}{dt}\sigma_{jk}(t) = -\frac{i}{\hbar}[\hat{V},\hat{\sigma}]_{jk} - \sum_\alpha \frac{P^\alpha}{M^\alpha}[\hat{d}^\alpha,\hat{\sigma}]_{jk}, \tag{3}$$

where $\sigma_{ij} = c_i cj^*$.

The third and final part of the propagation algorithm in FSSH is to allow for hops between surfaces. At every time

step, each trajectory has the ability to switch surfaces, thus forcing the relative number of trajectories on each surface to match approximately the probability density on that surface calculated according to the electronic wavefunction. In order to maintain this consistency, the probability for a hop during each time step, dt, from the current surface (call it i) to an alternative surface j can be no smaller than

$$\gamma_{ij}^{hop} = dt \left(\frac{2}{\hbar} \mathrm{Im}(c_j{}^* c_i V_{ji}) - 2\mathrm{Re}(c_j{}^* c_i \dot{\vec{R}} \cdot \vec{d}_{ji}) \right) \Big/ |c_i|^2. \tag{4}$$

Equation (4) is Tully's fewest switches criterion. Note that since we use an adiabatic basis, $V_{ji} = 0$ when $i \neq j$, and all hops are due to the derivative coupling in Eq. (4). If a hop does occur, then according to FSSH, the last step is to adjust the nuclear momentum in order to conserve energy.

By looking at Eqs. (2) and (4) it is possible to determine in what situations hops will occur. Equation (2) shows that if a trajectory is in a region of negligible derivative coupling, its associated electronic amplitude will not change. Once the trajectory enters a region of derivative coupling, however, the electronic amplitudes do change and hopping can occur. After leaving the region of derivative coupling, the hopping probability is again negligible. Therefore, for an FSSH calculation, the nuclei evolve classically in regions of negligible derivative coupling, and nuclei have the ability to switch surfaces only in regions of finite derivative coupling.

The asymmetric treatment of the nuclei and electrons described in this section leads to the decoherence problem, which standard FSSH does not address. We employ Sec. III B to explicitly define the decoherence problem, and discuss its origins.

B. Decoherence of the electronic density matrix and surface hopping

As it appears in the FSSH algorithm, the decoherence problem manifests itself in two complementary ways, one from the perspective of the electronic wavefunction and one from the perspective of the electronic density matrix. While wavefunctions and density matrices offer equivalent information in closed systems, they offer different perspectives for open quantum systems. We will describe the decoherence problem from both angles.

By design, the FSSH algorithm propagates a swarm of trajectories to approximate the density of a quantum wave packet in phase space. From the perspective of the electronic wavefunction, each individual FSSH trajectory is overcoherent and requires decoherence. To see this point, consider the electronic wavefunction for a trajectory that has just passed through a region of derivative coupling. After the trajectory has gone through the coupling region, the classical particle has either hopped or not hopped between surfaces. Of course, according to exact quantum dynamics, both possibilities occur at the same time, and the total nuclear-electronic wavefunction is really a superposition of wave packets on both surfaces. To account for this quantum superposition, FSSH stores a phase between the quantum wave packets in a simple electronic wavefunction (even though the classical particle is only moving along a single surface). Each FSSH trajectory carries its own electronic wavefunction and phase, in addition to position and momentum, altogether offering a global approximation to the exact phase that depends on nuclear position. The decoherence problem then arises after an avoided crossing event when wave packets separate on different surfaces, but each FSSH wavefunction retains its phase indefinitely, as if a superposition still exists at a point in R-space. The immediate consequence of this overcoherence is that the active surface populations and the weighted averages of the electronic wavefunction often no longer match. In the long run, this overcoherence problem is amplified by passing through regions of derivative coupling multiple times.[9,15–17,34,35] Eventually, after passing multiple times through a region of derivative coupling, the electronic wavefunction stored by FSSH corresponds to an ever more complicated (often completely nonsensical) superposition of wave packets.

The simplest solution to the overcoherence of the FSSH electron wavefunction is to remove the electronic component associated with the inactive surface.[15,20] Thus, after the trajectory has left the coupling region, the electronic wavefunction should be projected (or "collapsed") onto the active adiabatic surface, and the overcoherence problem can be solved by making the electronic wavefunction consistent with the active surface. The difficulty, however, is developing a consistent rule for knowing when to collapse the electronic wavefunction. For the simple decoherence criterion used in Ref. 36, we chose to collapse the electronic wavefunction at the minimum of the diabatic surfaces. Other authors have proposed to collapse the electronic wavefunction when the derivative coupling is below some threshold,[15] when trajectories diverge,[20] or when other heuristic measures apply.[28]

The A-FSSH algorithm (presented below) focuses on $\hbar$ and the difference in potential energy between the wave packets, evaluating that difference both at the current position of the surface hopping trajectory and at the fictitious position of the emerging wave packet. Ultimately, a successful algorithm for decoherence must collapse the wavefunction outside the region of derivative coupling, removing the overcoherence of the FSSH electronic wavefunction.

We can also view the decoherence problem from the perspective of the electronic density matrix. For a fully quantum system with two electronic states and one nuclear degree of freedom, the full density matrix $\hat{\boldsymbol{\rho}}$ at one point in position space is

$$\langle R|\hat{\boldsymbol{\rho}}|R\rangle = \begin{pmatrix} |\chi_1(R,t)|^2 & \chi_1(R,t)\chi_2^*(R,t) \\ \chi_2(R,t)\chi_1^*(R,t) & |\chi_2(R,t)|^2 \end{pmatrix}, \tag{5}$$

where $\chi_1(R,t)$ and $\chi_2(R,t)$ are the nuclear wavefunctions corresponding to the two electronic states. Tracing over the nuclear degrees of freedom gives the reduced electronic density matrix

$$\hat{\sigma} = \begin{pmatrix} \int dR|\chi_1(R,t)|^2 & \int dR\chi_1(R,t)\chi_2^*(R,t) \\ \int dR\chi_2(R,t)\chi_1^*(R,t) & \int dR|\chi_2(R,t)|^2 \end{pmatrix}. \tag{6}$$

At time $t = 0$, consider a nuclear wave packet moving towards an avoided crossing with all of its probability in the first electronic state ($\chi_2(R, t) = 0$). It is clear from Eq. (6) that the reduced electronic density matrix is initially pure ($\mathrm{Tr}(\hat{\sigma}^2) = 1$). After the system has passed through the avoided crossing, probability density will have moved from the first electronic state to the second electronic state, and our system will now be in a superposition of the two electronic states (i.e. both $\int dR|\chi_1(R, t)|^2 > 0$ and $\int dR|\chi_2(R, t)|^2 > 0$). So long as $\chi_1(R, t)$ and $\chi_2(R, t)$ differ by more than a constant factor, one can show that $\hat{\sigma}$ must be mixed ($\mathrm{Tr}(\hat{\sigma}^2) < 1$). At this point in time, because the nuclear wave packets on the different surfaces feel different forces, there will be a tendency for the nuclear wave packets χ_1 and χ_2 to spread apart, thus causing σ_{12} to decrease while the diagonal elements of $\hat{\sigma}$ remain constant. Here we assume that the wave packets do not enter a coupling region again. In the end, the decreasing σ_{12} in combination with the constant diagonal elements of $\hat{\sigma}$ implies that the reduced electronic density matrix is becoming more and more mixed ($\mathrm{Tr}(\hat{\sigma}^2)$ is decreasing).[20,21] To make the situation even more complicated, after evolution to longer times, the off-diagonal elements of $\hat{\sigma}$ may increase due to the nuclear wave packets coming back together and constructively interfering. For a periodic system, the reduced density matrix might even oscillate between pure and mixed matrices.

Comparing this exact quantum dynamical behavior to the FSSH algorithm reveals the decoherence problem from the perspective of the electronic density matrix. Within the FSSH algorithm, we propagate a swarm of trajectories, each with a corresponding electronic wavefunction or pure density matrix. Then, in order to estimate the reduced electronic density matrix as the partial trace over the nuclear coordinates of the full density matrix, we compute the statistical average of all those pure density matrices (with each trajectory given equal weight). Inevitably the reduced density matrix will become more or less mixed because the quantum system in FSSH (i.e., the electrons) interacts with a classical bath (i.e., the nuclei). We stress, however, that the reduced electronic density matrix for standard FSSH cannot become mixed at the correct rate.

Standard FSSH cannot find the correct rate of decoherence or possible recoherence because the absolute value of the off-diagonal elements of the electronic density matrix is constant when $\hat{d} = 0$ (see Eq. (3)). As described above, after passing through a region of derivative coupling, the FSSH algorithm does not recognize that two wave packets can separate, nor that the exact electronic density matrix can depend strongly on nuclear position. By contrast, A-FSSH improves on this situation by using a rigorous equation of motion for the reduced electronic density matrix based on the Liouville equation, and extracting a decoherence rate. In other words, the A-FSSH method attempts to reconstruct a fully reduced electronic density matrix (averaged over R-space) by correcting the FSSH local density matrix at each point in R-space. Alas, the A-FSSH approach is still unable to capture recurrences. After all, to capture recoherences and the effects of multiple wave packets recombining, we would require that surface hopping trajectories be run in parallel, so that different trajectories could recombine, and this parallelism goes against the very spirit of independent surface hopping trajectories.

To sum up, FSSH interprets a swarm of multiple trajectories as representing a quantum wave packet in phase space, and if we average over trajectories, the off-diagonal elements of the density matrix need not decay in time, and if they do decay, the decay rate will usually be incorrect. According to A-FSSH, we can effectively model a quantum-classical system with correctly decaying off-diagonal elements, corresponding to a mixed state, by collapsing the electronic wavefunction when appropriate (approximating the separation of the exact wave packets). This picture of decoherence in the surface hopping algorithm has strong implications.

IV. AUGMENTED FEWEST SWITCHES SURFACE HOPPING

We now review the A-FSSH algorithm, including a step-by-step recipe to facilitate its use by interested readers. The exact details of the method have been minimally changed in this paper compared to Refs. 16 and 37 in order to (i) simplify the algorithm, (ii) extend the algorithm to the case of multiple electronic states, (iii) improve long-time results for the calculation of rates for the spin-boson model, the most intensive benchmark so far applied to A-FSSH. All changes are rather minor and do not significantly alter the results of previous benchmarks.[16,17,37]

A. A-FSSH Review

1. Moments and Liouville equation

According to A-FSSH, we model a decoherence rate by the decay of the off-diagonal element of the reduced electronic density matrix ($\hat{\sigma} = \mathrm{Tr}_N \hat{\boldsymbol{\rho}}$), which we expect phenomenologically to have an exponential form,

$$|\sigma_{ij}(t)| \propto \exp\left(-t/\tau_d^{ij}\right), \tag{7}$$

where τ_d^{ij} is the decoherence rate between surfaces i and j.[38] To compute τ_d^{ij} in the context of surface-hopping trajectories, we use a moment expansion of the type found in correlated electronic-ionic dynamics of Horsfield *et al.*[39,40] along with a linear approximation for the equation of motion of $\hat{\sigma}$; according to A-FSSH (and unlike FSSH), the magnitude of σ_{ij} may change outside regions of derivative coupling. One key difference between our approach and that of Horsfield *et al.* is that we expand the Liouville equation around a surface hopping trajectory ($R_{SH}(t)$, $P_{SH}(t)$) rather than an Ehrenfest trajectory.

In this paper we define our moments slightly differently than we have in previous A-FSSH publications.[16,37] Here, we define our position and momentum moments relative to the surface hopping trajectories as follows:

$$\delta\hat{R}^{\alpha}(t) \equiv \mathrm{Tr}_N\Big[\left(\mathbf{R}^{\alpha} - \left\langle R^{\alpha}_{SH}(t)\right|\mathbf{R}^{\alpha}\left|R^{\alpha}_{SH}(t)\right\rangle \mathbf{I}_N\right) \times \left(\hat{\boldsymbol{\rho}}(t) - \langle\Phi_{act}|\hat{\boldsymbol{\rho}}(t)|\Phi_{act}\rangle\hat{I}_e\right)\Big], \tag{8}$$

$$\delta\hat{P}^{\alpha}(t) \equiv \mathrm{Tr}_N\Big[\left(\mathbf{P}^{\alpha} - \left\langle P^{\alpha}_{SH}(t)\right|\mathbf{P}^{\alpha}\left|P^{\alpha}_{SH}(t)\right\rangle \mathbf{I}_N\right) \times \left(\hat{\boldsymbol{\rho}}(t) - \langle\Phi_{act}|\hat{\boldsymbol{\rho}}(t)|\Phi_{act}\rangle\hat{I}_e\right)\Big], \tag{9}$$

or employing the linearity of the partial trace

$$\Delta\hat{R}^{\alpha}(t) \equiv \mathrm{Tr}_N\left[\left(\mathbf{R}^{\alpha} - R^{\alpha}_{SH}(t)\right)\hat{\boldsymbol{\rho}}(t)\right], \tag{10}$$

$$\Delta\hat{P}^{\alpha}(t) \equiv \mathrm{Tr}_N\left[\left(\mathbf{P}^{\alpha} - P^{\alpha}_{SH}(t)\right)\hat{\boldsymbol{\rho}}(t)\right], \tag{11}$$

$$\delta\hat{R}^{\alpha}(t) = \Delta\hat{R}^{\alpha}(t) - \langle\Phi_{act}|\,\Delta\hat{R}^{\alpha}(t)\,|\Phi_{act}\rangle\,\hat{I}_e, \tag{12}$$

$$\delta\hat{P}^{\alpha}(t) = \Delta\hat{P}^{\alpha}(t) - \langle\Phi_{act}|\,\Delta\hat{P}^{\alpha}(t)\,|\Phi_{act}\rangle\,\hat{I}_e, \tag{13}$$

where $|\Phi_{act}\rangle$ is the state of the active surface, i.e., the surface that the surface-hopping trajectory is walking along. In Eqs. (8) and (9), we have shifted the position and momentum moments so that all moments on the active surface are always zero, $\delta R^{\alpha}_{act,act}(t) = \delta P^{\alpha}_{act,act}(t) = 0$. In doing so, we find simpler expressions relative to Ref. 16 for decoherence rates and a more natural extension to the case of multiple (i.e., more than two) electronic states.

We derive the equations of motion for the moments in Eqs. (8) and (9) by expanding the full quantum Liouville equation to first order in the moments (ignoring terms with second order derivatives of the potential energy) giving[16]

$$T^{R}_{jk} \equiv -\frac{i}{\hbar}[\hat{V}, \delta\hat{R}^{\alpha}]_{jk} + \frac{\delta P^{\alpha}_{jk}}{M^{\alpha}} - \sum_{\beta}\frac{P^{\beta}_{SH}}{M^{\beta}}[\hat{d}^{\beta}, \delta\hat{R}^{\alpha}]_{jk}, \tag{14}$$

$$\frac{d}{dt}\delta R^{\alpha}_{jk} = T^{R}_{jk} - T^{R}_{ii}\delta_{jk}, \tag{15}$$

$$T^{P}_{jk} \equiv -\frac{i}{\hbar}[\hat{V}, \delta\hat{P}^{\alpha}]_{jk} + \frac{1}{2}(\delta\hat{F}^{\alpha}\hat{\sigma} + \hat{\sigma}\delta\hat{F}^{\alpha})_{jk} - \sum_{\beta}\frac{P^{\beta}_{SH}}{M^{\beta}}[\hat{d}^{\beta}, \delta\hat{P}^{\alpha}]_{jk}, \tag{16}$$

$$\frac{d}{dt}\delta P^{\alpha}_{jk} = T^{P}_{jk} - T^{P}_{ii}\delta_{jk}, \tag{17}$$

where the active surface is the ith surface, $\hat{V} \equiv \hat{V}(\vec{R}_{SH}(t))$ is the matrix of potential energy surfaces, and $\hat{F}^{\alpha} \equiv \hat{F}^{\alpha}(\vec{R}_{SH}(t)) = -\partial\hat{V}/\partial R^{\alpha}|_{\vec{R}_{SH}}$ is the matrix of forces. We define the force difference $\delta\hat{F}^{\alpha} \equiv \hat{F}^{\alpha} - F^{\alpha}_{SH}\hat{I}_e$, where $\vec{F}_{SH}$ is the force on the active surface at $\vec{R}_{SH}$ ($F^{\alpha}_{SH} = -\partial V_{ii}/\partial R^{\alpha}|_{\vec{R}_{SH}}$).

The equation of motion for the reduced electronic density matrix is

$$\frac{d}{dt}\sigma_{jk}(t) = -\frac{i}{\hbar}[\hat{V}, \hat{\sigma}]_{jk} + \sum_{\alpha}\frac{i}{\hbar}[\hat{F}^{\alpha}, \delta\hat{R}^{\alpha}]_{jk} - \sum_{\alpha}\frac{P^{\alpha}_{SH}}{M^{\alpha}}[\hat{d}^{\alpha}, \hat{\sigma}]_{jk}. \tag{18}$$

Note that Eq. (18) is the same as Eq. (3) except for the $[\hat{F}^{\alpha}, \delta\hat{R}^{\alpha}]$ term. This additional term yields a correction to $\hat{\sigma}$. For our purposes, the off-diagonal corrections to $\hat{\sigma}$ are the most important as they allow us to calculate the decoherence rate.

2. Decoherence rate

Comparing Eq. (18) with Eq. (7), and assuming a region of zero derivative coupling ($\vec{d}_{ni} = 0$), we find a nominal decoherence rate (between wave packets on surfaces i and n)

$$\frac{1}{\tau^{ni}_{d}} = -\frac{\frac{d}{dt}|\sigma_{ni}(t)|}{|\sigma_{ni}(t)|} = -\frac{\frac{d}{dt}|\sigma_{ni}(t)|^2}{2|\sigma_{ni}(t)|^2} = \mathrm{Im}\sum_{\alpha}\left(\frac{\left(F^{\alpha}_{nn} - F^{\alpha}_{ii}\right)\delta R^{\alpha}_{ni}}{\hbar\sigma_{ni}}\right). \tag{19}$$

This expression is not stable, however, since σ_{ni} can get quite small and it is in the denominator of Eq. (19). To derive a stable rate, we assume a frozen Gaussian[41] form for the nuclear wavefunctions, with our total wavefunction as

$$\langle\vec{r}, \vec{R}|\Psi(t)\rangle \approx \sum_{k} c_k g_k(\vec{R})\langle\vec{r}|\Phi_k(\vec{R})\rangle, \tag{20}$$

where

$$g_k(\vec{R}) \equiv \langle\vec{R}|g_k(\vec{R}_k, \vec{P}_k)\rangle \tag{21}$$

$$\equiv \prod_{\alpha}\left(\frac{1}{\pi a_{R^{\alpha}}{}^2}\right)^{\frac{1}{4}}\exp\left(\frac{-\left(R^{\alpha} - R^{\alpha}_{k}(t)\right)^2}{2a_{R^{\alpha}}{}^2}\right) \tag{22}$$

$$\times\exp\left(\frac{i}{\hbar}P^{\alpha}_{k}(t)(R^{\alpha} - R^{\alpha}_{k}(t))\right). \tag{23}$$

In this approximation, the total wavefunction is a superposition of multiple Gaussian wave packets, one on each surface and each with an associated time-dependent position and momentum ($\vec{R}_k(t)$, $\vec{P}_k(t)$). With this simplification, we can approximate the relevant term in Eq. (19) by carrying out the nuclear traces as integrals over the nuclear coordinates giving

$$\mathrm{Im}\left(\frac{\delta R^{\alpha}_{ni}}{\sigma_{ni}}\right) \approx \left(\frac{\left(P^{\alpha}_{n} - P^{\alpha}_{i}\right)a_{R^{\alpha}}{}^2}{2\hbar}\right). \tag{24}$$

This still does not give a unique expression for the decoherence rate, however, because we have not defined a width of the Gaussians, $a_{R^{\alpha}}$. To that end, we choose the widths in order to maximize the overlap of the wave packets on the two relevant surfaces (the ith and the nth as written). In other words, we require

$$\frac{\partial|\langle g_n|g_i\rangle|}{\partial a_{R^{\alpha}}} = 0, \tag{25}$$

which gives

$$a_{R^{\alpha}}{}^2 = \hbar\frac{|R^{\alpha}_{n} - R^{\alpha}_{i}|}{|P^{\alpha}_{n} - P^{\alpha}_{i}|}. \tag{26}$$

This choice should result in a minimal rate of collapsing events that still satisfies the correct decay of the off-diagonal matrix element in Eq. (19).

Finally, we plug Eq. (26) back into Eqs. (19) and (24), identifying the Gaussian wavepacket centers as

$$R^{\alpha}_{n} \approx R^{\alpha}_{SH}(t) + \frac{\delta R^{\alpha}_{nn}}{\sigma_{nn}}, \tag{27}$$

with $R_i^\alpha = R_{SH}^\alpha$ by definition (i is always our label for the active surface), and we compute

$$\frac{1}{\tau_d^{ni}} = \sum_\alpha \frac{\left(F_{nn}^\alpha - F_{ii}^\alpha\right)\delta R_{nn}^\alpha}{2\hbar\sigma_{nn}}. \tag{28}$$

Here we assume $\mathrm{sgn}(\delta R_{nn}^\alpha) = \mathrm{sgn}(\delta P_{nn}^\alpha)$ so that wave packets have just recently separated, consistent with these moments being small and a short time approximation. Because the σ_{nn} term can be problematic (in the denominator), again we preserve the theme of having the fewest number of collapsing events, and we choose the maximal value for the electronic density matrix, $\sigma_{nn} = 1$:

$$\frac{1}{\tau_d^{ni}} = \sum_\alpha \frac{\left(F_{nn}^\alpha - F_{ii}^\alpha\right)\delta R_{nn}^\alpha}{2\hbar}. \tag{29}$$

3. Decoherence in regions of derivative coupling

The derivation of our decoherence rate has relied so far on the approximation that the derivative coupling is negligible. Of course this is not always true, and our treatment of the decoherence rate must be slightly modified for accuracy, especially within regions of derivative coupling. After all, the idea behind A-FSSH is that after the trajectory has left a region of derivative coupling, the electronic wavefunction must collapse onto the current surface in order to correct for the overcoherence of FSSH. However, collapsing inside a region of derivative coupling is a bad idea leading to spurious results.[42] To discourage collapses in regions of derivative coupling, we reduce our decoherence rate by a factor that arises from Eq. (18) for non-zero derivative couplings. In that case, the off-diagonal term of the force matrix is nonzero and satisfies

$$F_{ni}^\alpha = d_{ni}^\alpha \left(E_n(R) - E_i(R)\right). \tag{30}$$

These non-zero derivative couplings result in an extra term in Eq. (19)

$$\mathrm{Im}\sum_\alpha \left(\frac{F_{ni}^\alpha\left(\delta R_{ii}^\alpha - \delta R_{nn}^\alpha\right)}{\hbar\sigma_{ni}}\right). \tag{31}$$

In order to estimate an average magnitude for σ_{ni} we take $|\sigma_{ni}| \approx \sqrt{\sigma_{nn}\sigma_{ii}}$ to have its maximum value with $\sigma_{nn} = \sigma_{ii} = \frac{1}{2}$ so that $\mathrm{Im}(\sigma_{ni}) \approx \frac{1}{2}$ in Eq. (31). We then subtract the absolute value of Eq. (31) from the total decoherence rate. In this way, the additional term serves as an impediment to collapsing in regions of derivative coupling. This gives the final decoherence rate that we use in A-FSSH for separation of the wave packet on an inactive surface n and the wave packet on an active surface i,

$$\text{(final expression)}\quad \frac{1}{\tau_d^{ni}} \equiv \sum_\alpha \frac{\left(F_{nn}^\alpha - F_{ii}^\alpha\right)\delta R_{nn}^\alpha}{2\hbar} - \frac{2\left|\sum_\alpha F_{in}^\alpha \delta R_{nn}^\alpha\right|}{\hbar}\zeta, \tag{32}$$

where $\zeta = 1$. Again, i is the active surface, so $\delta R_{ii} = 0$.

The choice of $\mathrm{Im}(\sigma_{ni}) = \frac{1}{2}$ in Eq. (31) is an approximation that leads to $\zeta = 1$ in Eq. (32), but we can test our choice with a simple model. The magnitude of ζ controls the collapse or decoherence rates of A-FSSH. Larger values of ζ will result in less decoherence both within and outside the regions of derivative coupling. In order to decide on the right amount of decoherence we need a model that is sensitive to how much decoherence is added. For this purpose, we use a narrow avoided crossing as shown in Fig. 1.[17,43] Figure 2 shows the probability of being reflected on the lower adiabatic surface as a function of initial momentum. The exact result shows oscillations in this probability due to quantum resonances. Standard FSSH shows oscillations as well, but the oscillations are far too numerous and wild compared with the exact results. The first panel in Fig. 2 shows that the choice of $\zeta = 1$ in Eq. (32) produces oscillations that are most similar to the exact result. $\zeta < 1/2$ leads to more decoherence, resulting in fewer and smaller oscillations. $\zeta > 2$ results in too little

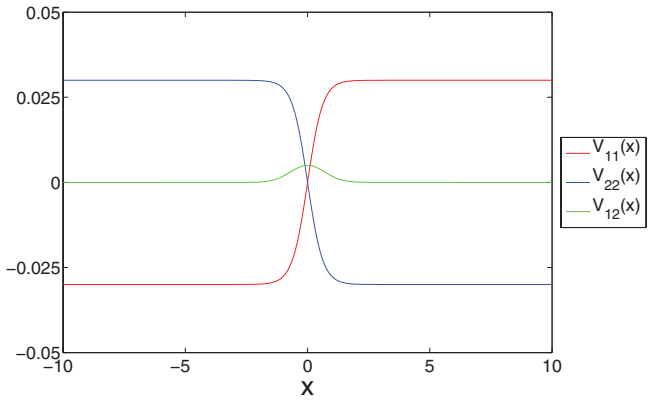

FIG. 1. Avoided crossing used for the reflection probabilities in Figure 2 to test our collapse rate (in Eq. (32)) in the vicinity of an avoided crossing. For details of the potential energy surfaces, see Ref. 43.

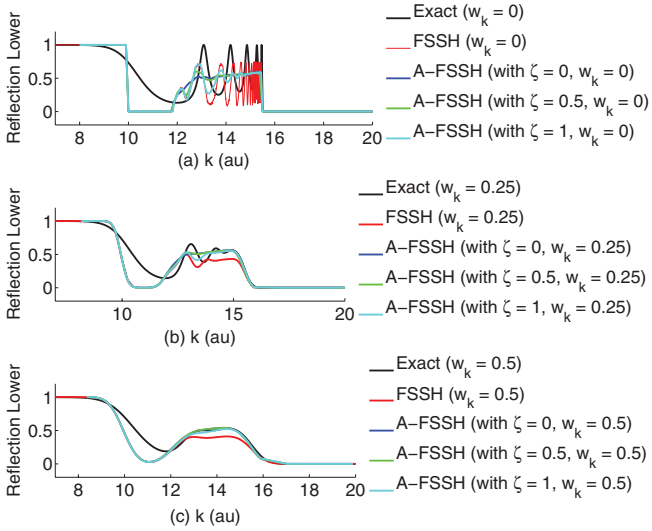

FIG. 2. Probability of reflection on the lower surface as a function of initial momentum. Here, we compare the exact answer with both FSSH results and A-FSSH results for differing amounts of decoherence (i.e., different values of ζ in Eq. (32)). (a) We compare quantum plane-wave scattering calculations and surface hopping trajectories with fixed initial momentum. (b) and (c) We compare quantum wave packet scattering with initial width $w_k = 1/(\sqrt{2}a_R)$ in momentum space (see Eq. (22) for a definition of a_R) and surface hopping dynamics averaged over the same width. Note that $\zeta = 1$ appears optimal.

decoherence and its probability of reflection on the lower surface is essentially identical to that from standard FSSH (not shown). The second and third panels in Fig. 2 show results from quantum wave packet and surface-hopping calculations, where the latter are averaged over initial positions with the same width as the corresponding wave packets in the former. The decoherence rate in Eq. (32) (with $\zeta = 1$) proves to give the best results.

4. Resetting the moments: Failure of the linear approximation

We chose a constant value for σ_{ni} in Eq. (31) in order to ensure the stability of our algorithm. In fact, several of our algorithmic choices thus far have had this objective in mind, but the algorithm is still not completely stable in its current form. Our final remaining problem is the robustness of the moments. Although, the moments $\delta\hat{R}$ and $\delta\hat{P}$ give a good indication of how wave packets separate, they still obey equations of motion based on a linearized approximation and are not perfectly stable; they can lose their meaning at long times. To increase the stability of the algorithm further we must allow the moments to be reset. If forces on the different surfaces tend to push wave packets apart, then decoherence events are possible and we must keep track of the moments and relative motion on different surfaces. However, if the forces tend to pull wave packets together, the moments become both less meaningful and less useful, and we believe they can and should be safely reset. By similar reasoning to what we used to derive Eq. (32), the rate that we reset the moments should be the negative collapsing rate without the extra fluctuation term. Explicitly we propose to reset the moments with rate

$$\frac{1}{\tau_r^{ni}} = -\sum_\alpha \left(\frac{\left(F_{nn}^\alpha - F_{ii}^\alpha\right)\delta R_{nn}^\alpha}{2\hbar} \right). \tag{33}$$

In the end, using Eqs. (32) and (33) we can be confident that all moments, $\delta\hat{R}$ and $\delta\hat{P}$, will always be small, and therefore a linearized equation-of-motion should be meaningful and the A-FSSH algorithm should be accurate.

B. A-FSSH step-by-step algorithm

We now present a step-by-step algorithm of our A-FSSH method in order to be as clear as possible. This algorithm is written for N electronic states and any number of nuclear dimensions even though in this paper we apply it to the spin-boson model in one nuclear dimension for two electronic states. We have successfully tested the algorithm on problems involving three electronic states.[37]

1. As in standard FSSH, we initialize a mixed quantum-classical trajectory by fixing the initial classical coordinates $\vec{R}_0$ and $\vec{P}_0$ and electronic wavevector $\vec{c}_0$ at time $t = 0$. We start on a specific adiabatic surface, which for the purpose of this algorithm we call the ith surface. As for the moments, we set $\delta\hat{R} = \delta\hat{P} = 0$.
2. To go from time t to $t + dt$, we propagate our dynamical variables.
   (a) For the nuclear coordinates, as in standard FSSH, we propagate $\vec{R}$ and $\vec{P}$ according to Newton's laws
   $$\frac{dR^\alpha}{dt} = \frac{P^\alpha}{M^\alpha}, \tag{34}$$
   $$\frac{dP^\alpha}{dt} = F_{ii}^\alpha(\vec{R}). \tag{35}$$
   (b) We propagate the electronic amplitude $\vec{c}$ according to Eq. (2) (just as in FSSH).
   (c) Unique to A-FSSH, we propagate the moments $\delta\hat{R}$ and $\delta\hat{P}$ according to Eqs. (14)–(17).
3. As in standard FSSH, while the nuclei are being propagated along the ith adiabatic electronic surface, at each time step, we evaluate the probability to switch to any other state (labeled $j \neq i$, for instance) $\gamma_{\text{hop}}^{i\to j}$. This switching probability is chosen to be as small as possible, while still forcing the relative populations on the different surfaces to match the norm of the electronic amplitudes. Tully has shown[5] in a straightforward manner that, in a simulation time step dt, the rate is
   $$\gamma_{\text{hop}}^{i\to j} = -\sum_\alpha \frac{2P^\alpha}{M^\alpha} \frac{\text{Re}\left(d_{ji}^\alpha(\vec{R})c_i c j^*\right)}{|c_i|^2} dt. \tag{36}$$
   In order to implement this hopping criterion with a single pseudorandom number $\zeta \in [0, 1]$ for each time step, we form the array
   $$S_j = \sum_{l\le j} \gamma_{\text{hop}}^{i\to l}. \tag{37}$$
   We set $S_0 \equiv 0$ by definition and we know that $S_N = \gamma_{\text{tot}}$ is the total probability of hopping. Also since $\gamma_{\text{hop}}^{i\to i} = 0$ we have $S_i = S_{i-1}$.
   (a) If $\zeta > \gamma_{\text{tot}}$ then we do not hop and continue to step 6.
   (b) If $\zeta < \gamma_{\text{tot}}$ then there will be a hopping event to surface j if it is energetically allowed where j is determined from $S_{j-1} < \zeta < S_j$. We determine if the hop is allowed in step 4.
4. As in standard FSSH, in order to maintain conservation of energy when moving from the ith to the jth adiabatic potential energy surface, we compute a rescaled nuclear momentum on the new surface in a direction $\vec{u}_{sc}$ chosen to be in the direction of derivative coupling $\vec{u}_{sc} = \vec{d}_{ij}$. We determine the new momentum $\vec{P}^{\text{new}}$ from
   $$\vec{P}^{\text{new}} = \vec{P} + \kappa\vec{u}_{sc}, \tag{38}$$
   $$\sum_\alpha \frac{(P^{\alpha,\text{new}})^2}{2M^\alpha} + V_{jj}(\vec{R}) = \sum_\alpha \frac{(P^\alpha)^2}{2M^\alpha} + V_{ii}(\vec{R}). \tag{39}$$
   Equations (38) and (39) result in a quadratic equation for κ with two roots in general. We choose the root with the smaller $|\kappa|$. Other choices of rescaling direction ($\vec{u}_{sc}$) are possible.[12,37]

(a) If hopping to the new state is forbidden by energy conservation ($\vec{P}^{\text{new}}$ is complex) we do not hop and continue with step 6.
(b) If the new hop is allowed ($\vec{P}^{\text{new}}$ is real) we hop and continue with step 5.

5. Given that a hop will now occur, we must adjust the dynamical variables.
   (a) We rescale the momentum, $\vec{P} = \vec{P}^{\text{new}}$, according to Eqs. (38) and (39).
   (b) We reset the position moment, $\delta\hat{R} = 0$.
   (c) For each electronic state k, we force the diagonal element of the momentum moment to obey conservation of energy

$$\delta P_{kk}^{\alpha,\text{new}} = \eta_k u_{sc}^{\alpha}, \tag{40}$$

$$\sum_{\alpha} \frac{\left(P^{\alpha,\text{new}} + \frac{\delta P_{kk}^{\alpha,\text{new}}}{\sigma_{kk}}\right)^2}{2M^{\alpha}} + V_{kk}(\vec{R}) = E_{\text{tot}}, \tag{41}$$

   for each k with

$$E_{\text{tot}} = \sum_{\alpha} \frac{(P^{\alpha,new})^2}{2M^{\alpha}} + V_{jj}(\vec{R}). \tag{42}$$

   If there are two real roots to Eqs. (40) and (41), we choose the η_k with the smallest absolute value. If any new diagonal element of $\delta\hat{P}$ as given by Eqs. (40) and (41) is complex then that element is set to zero. We set the off-diagonal elements of $\delta\vec{P}$ to zero. Before solving for η_k, we multiply Eq. (41) by σ_{kk}^2 so that if $\sigma_{kk} = 0$ we end up with $\delta\vec{P}_{kk} = 0$.
   (d) For the purposes of this enumerated algorithm we switch the labels of the electronic surfaces i and j so that we are again walking on the ith surface, and we continue onto step 6.

6. For each component of the electronic wavevector c_n with $n \neq i$, we determine the probability of collapse, $\gamma_n^{\text{collapse}}$, using the decoherence rate from Eq. (32). For the time interval dt we have

$$\gamma_n^{\text{collapse}} = dt\frac{1}{\tau_d^{ni}}. \tag{43}$$

   We also check to see whether the moments should be reset using the rate in Eq. (33) to give the reset probability

$$\gamma_n^{\text{reset}} = dt\frac{1}{\tau_r^{ni}}. \tag{44}$$

   (Note: it is never possible to both collapse and reset with respect to the same surface during the same time step because if $\frac{1}{\tau_d^{ni}}$ is positive, then $\frac{1}{\tau_r^{ni}}$ must be negative.)
   (a) To check for collapsing events onto each surface we loop over n.
      i. For each state $n \neq i$ we generate a random number $\eta_n \in [0, 1]$.
      ii. If $\eta_n > \gamma_n^{\text{collapse}}$, then we do not have a collapsing event for that state.
      iii. If $\eta_n < \gamma_n^{\text{collapse}}$, then we have a collapsing event and the electronic amplitude on state n becomes 0. The electronic amplitudes become

$$c_j^{\text{new}} = \begin{cases} c_j/\mu & j \neq n \\ 0 & j = n \end{cases} \qquad \mu = \sqrt{1 - |c_n|^2}. \tag{45}$$

      iv. If we have a collapsing event, all elements of the moments associated with state n are set to zero. We end up with

$$\delta\vec{R}_{jn} = \delta\vec{R}_{nj} = 0 \text{ for all } j, \tag{46}$$

$$\delta\vec{P}_{jn} = \delta\vec{P}_{nj} = 0 \text{ for all } j. \tag{47}$$

      v. Similarly, if $\eta_n > \gamma_n^{\text{reset}}$, then we do not have a resetting event.
      vi. If $\eta_n < \gamma_n^{\text{reset}}$, then we reset all position and momentum moments associated with the nth electronic state to zero just as in Eqs. (46) and (47). This is the end of the loop over n.
   (b) We return to step 2 and continue the algorithm.

V. SPIN-BOSON MODEL

A. Potential energy surfaces

The spin-boson model has been widely used to study electron transfer.[7,14,44–47] It gives us an important benchmark for surface-hopping algorithms because it is a simple two level system that can provide a stringent test by looking at the rate of relaxation into one diabatic well from the other well. For our purposes, the key point is that a typical trajectory crosses many times through the region of derivative coupling.

The spin-boson model consists of two parabolic diabatic electronic states coupled by a constant off-diagonal diabatic coupling term. The most general possible Hamiltonian (written in the diabatic basis $\{|\Xi_l\rangle, |\Xi_r\rangle\}$) is therefore

$$H = \begin{pmatrix} \frac{1}{2}m\omega^2x^2 + Mx & V \\ V & \frac{1}{2}m\omega^2x^2 - Mx - \epsilon_0 \end{pmatrix}. \tag{48}$$

Diagonalizing the Hamiltonian (48) gives the adiabatic energy surfaces as well as the derivative coupling. They are

$$E_1(x) = \frac{1}{2}m\omega^2x^2 - \frac{\epsilon_0}{2} - \sqrt{\left(\frac{\epsilon_0}{2} + Mx\right)^2 + V^2}, \tag{49}$$

$$E_2(x) = \frac{1}{2}m\omega^2x^2 - \frac{\epsilon_0}{2} + \sqrt{\left(\frac{\epsilon_0}{2} + Mx\right)^2 + V^2}, \tag{50}$$

and

$$d_{12}(R) = \frac{1}{2}\frac{MV}{(Mx + \epsilon_0/2)^2 + V^2}. \tag{51}$$

The eigenvectors of the Hamiltonian (48) give the adiabatic states in terms of the original diabatic states

$$|\Phi_1(x)\rangle = f_1(x)|\Xi_l\rangle + g_1(x)|\Xi_r\rangle, \tag{52}$$

$$|\Phi_2(x)\rangle = f_2(x)|\Xi_l\rangle + g_2(x)|\Xi_r\rangle, \tag{53}$$

where

$$f_1(x) = \sqrt{\frac{1}{2} - \frac{1}{2}\frac{Mx + \epsilon_0/2}{\sqrt{(Mx + \epsilon_0/2)^2 + V^2}}}, \tag{54}$$

$$g_1(x) = -\sqrt{\frac{1}{2} + \frac{1}{2}\frac{Mx + \epsilon_0/2}{\sqrt{(Mx + \epsilon_0/2)^2 + V^2}}}, \tag{55}$$

$$f_2(x) = \sqrt{\frac{1}{2} + \frac{1}{2}\frac{Mx + \epsilon_0/2}{\sqrt{(Mx + \epsilon_0/2)^2 + V^2}}}, \tag{56}$$

$$g_2(x) = \sqrt{\frac{1}{2} - \frac{1}{2}\frac{Mx + \epsilon_0/2}{\sqrt{(Mx + \epsilon_0/2)^2 + V^2}}}. \tag{57}$$

As we will discuss in Sec. V C, the coefficients $f_i(x)$ and $g_i(x)$ are necessary to convert between adiabatic and diabatic states. We will be interested in populations on and rates between diabatic states even though the actual calculations are carried out in an adiabatic basis. It is necessary, therefore, to convert a trajectory on one adiabatic surface into an expectation value of being on either diabatic surface using these coefficients.

The convenience of the spin-boson model is that, in the transition state frictional regime, the transition rate is well known. It is given at high temperature by the Marcus rate[48]

$$k_{l\to r} = \frac{2\pi |V|^2}{\hbar\sqrt{4\pi E_r kT}} \exp\left(-\frac{(E_r - \epsilon_0)^2}{4E_r kT}\right), \tag{58}$$

which is derived from second order perturbation theory.[49] This gives us an exact rate against which we can compare results.

B. Parameter regimes

For the spin-boson model, there are six relevant energy scales: the reorganization energy $E_r = 2\frac{M^2}{m\omega^2}$, the temperature kT, the driving force ϵ_0 (sometimes denoted ΔG), the diabatic coupling V, the frequency of the electronic potential energy surfaces $\hbar\omega$, and the friction coefficient $\hbar\gamma$. The diabatic coupling V is especially important in our analysis because it determines the adiabaticity of our system. In particular, the Hamiltonian is considered to be in the nonadiabatic regime if the diabatic coupling V is "small" (defined later) and in the adiabatic regime if V is "large."

A small diabatic coupling results in trajectories that pass through the coupling region several times before relaxing into a separate diabatic well, and as we have discussed above, multiple passes through the coupling region amplifiy FSSH's decoherence problem. For this reason, the nonadiabatic regime offers the surface-hopping method its most stringent test. The parameter that determines whether the system is in the adiabatic or nonadiabatic regime is the Landau-Zener parameter $\alpha_{LZ} = \frac{2\pi V^2}{\hbar\dot{R}|F_b - F_a|}$, where F_a and F_b are the forces on the two surfaces at the crossing point.[49] In our case of harmonic surfaces, assuming a Maxwell-Boltzmann velocity, we estimate $\alpha_{LZ} = \frac{2\pi V^2}{\hbar\omega\sqrt{2kTE_r}}$. The nonadiabatic regime is given by $\alpha_{LZ} \ll 1$, meaning that V must be small.

Having insisted on a small diabatic coupling, we would also like to be in the transition state frictional regime, where Eq. (58) can be used as a point of comparison. To that end, in our calculations, γ should not be too large or too small.[49,50] On the one hand, if γ is too large, the dynamics are diffusive and we are in the overdamped limit. On the other hand, if γ is too small, the nuclei may no longer be in thermal equilibrium, and we are in the underdamped limit. As is well known, to be in the transition state limit we must have not only a Maxwell-Boltzmann thermal distribution of momentum at the crossing point, but also ballistic rather than diffusive dynamics at the crossing point.[49]

Now, maintaining a thermal distribution on one adiabatic state imposes constraints on the electronic transtion rate between states. Specifically, for thermal equilibrium, we require that relaxation within one state must take place faster than electronic transitions to another state, so that $\gamma \gg \frac{V^2}{\sqrt{E_r kT}}$. This places a lower limit on γ. At the same time, whether a system obeys ballistic or diffusive escape dynamics is decided by the characteristic time each trajectory spends in the coupling region versus the friction timescale. The timescale that a trajectory spends in the coupling region can be estimated as the width of the derivative coupling region, $\frac{V}{M} = \sqrt{\frac{2V^2}{E_r m\omega^2}}$ divided by the average speed of the trajectory $\sqrt{\frac{kT}{m}}$. Comparing the result with the timescale for the friction γ, we find the condition $\frac{\sqrt{E_r kT}\omega}{V} \gg \gamma$. This places an upper limit on γ. In the end, we have at least two necessary conditions for the transition state frictional regime: $\frac{\sqrt{E_r kT}\omega}{V} \gg \gamma \gg \frac{V^2}{\sqrt{E_r kT}}$.

C. Numerical methods

In this paper, we compare transition rates for the spin-boson model according to standard Tully-style FSSH (Ref. 5) (as in Sec. III) and A-FSSH (as in Sec. IV). We also compare these rates with a simple phenomenological model that adds decoherence to FSSH (henceforth denoted "simple collapse").[36] For the simple collapse method, we propagate FSSH trajectories but we collapse the electronic wavefunction whenever the particle crosses the minimum of a diabatic well while moving away from the crossing point. More explicitly, for the normal Marcus regime, we set the electronic wavefunction to $\binom{1}{0}$ each time the position of a trajectory crosses $x = \pm\frac{M}{m\omega^2}$ while moving on the lower surface headed away from the crossing region. For the inverted regime, simple collapses occur on the upper surface for $x = -\frac{M}{m\omega^2}$ and on the lower surface for $x = \frac{M}{m\omega^2}$. This collapsing criterion was roughly suggested by Fang and Hammes-Schiffer.[15] The reasoning is quite sensible: once a trajectory is far from the crossing region, wave packets on the upper and lower surface should separate, there is no longer a possibility to hop, and the particle should "forget" that it was ever in the crossing region. The simple collapse method essentially has the correct decoherence behavior and is included because it serves as a point of reference for A-FSSH. Note that A-FSSH is preferable to simple collapse in general because (i) A-FSSH can be used over the entire range of ϵ_0, including the normal, inverted, and barrierless regimes; (ii) A-FSSH can be used even when

the shape of the entire surface is not known *a priori* (unlike simple collapse).

Although we carry out all surface-hopping dynamics on the adiabatic surfaces given by Eqs. (49) and (50), we need to calculate the transition rate between diabatic states. Thus, it is necessary to convert a trajectory moving along one of the adiabatic surfaces into a probability of being on one of the diabatic surfaces. To do this, we use the coefficients $f_i(x)$ and $g_i(x)$ from Eqs. (54)–(57) together with the following natural interpretation: if one is moving along the bottom (active) adiabatic surface corresponding to $|\Phi_1(x)\rangle$, we assume that the probability of being on the left diabatic is $|f_1(x)|^2$ and the probability of being on the right is $|g_1(x)|^2$. Similarly, if the upper adiabatic surface is the active surface, corresponding to $|\Phi_2(x)\rangle$, we take that the probability of being on the left diabatic to be $|f_2(x)|^2$ and the probability of being on the right is $|g_2(x)|^2$.

In order to simulate the system at finite temperature we consider our system to be in contact with a classical thermal bath through the nuclear coordinate. We model this contact by adding a random force ξ and friction term γ yielding a form of Langevin dynamics, following the work of Tully and Beeman.[51,52] For each of the methods we study, we propagate the nuclear trajectories along the adiabatic surfaces given by Eqs. (49) and (50) with the additional forces due to the bath. At each time step, the total force on the nuclear degree of freedom is therefore

$$F = -\frac{dE_i(x)}{dx} - \gamma p + \xi, \tag{59}$$

where i is the label of the active surface that the trajectory is moving along and ξ is a Markovian Gaussian random force with standard distribution $\sigma = \sqrt{2\gamma mkT/dt}$ (with time step dt). For the discrete integration of the equations of motion, the Markov property means that the force at each time step is uncorrelated with the force at the previous time step.

To capture the Marcus transition rates we needed to simulate the system starting at equilibrium in the left diabatic well and transitioning to the other well. Thus, we used a Boltzmann distribution of nuclear positions and a Maxwell-Boltzmann distribution of momenta in the left diabatic well as our initial coordinates. We used the initial positions and diabatic surface of each particle to calculate both the probability of being on either adiabatic surface (i.e., choosing the active surface) and also the electronic wavefunction (in the adiabatic basis). In choosing the phase of the electronic wavefunction, we elected to make each component real. Specifically, the electronic wavefunction for a trajectory starting at position x was given by

$$\begin{pmatrix} \sqrt{\frac{1}{2} - \frac{1}{2}\frac{Mx+\epsilon_0/2}{\sqrt{(Mx+\epsilon_0/2)^2+V^2}}} \\ \sqrt{\frac{1}{2} + \frac{1}{2}\frac{Mx+\epsilon_0/2}{\sqrt{(Mx+\epsilon_0/2)^2+V^2}}} \end{pmatrix} \tag{60}$$

and the probability of choosing the lower adiabatic surface as the active surface was

$$\frac{1}{2} - \frac{1}{2}\frac{Mx+\epsilon_0/2}{\sqrt{(Mx+\epsilon_0/2)^2+V^2}}. \tag{61}$$

TABLE I. Energy regimes and ranges used for surface hopping calculations ($\hbar = 1$).

Parameter	Range
E_r	2.39×10^{-2}
kT	9.5×10^{-4}
ϵ_0	1.8×10^{-2}–3.0×10^{-2}
V	1.25×10^{-5}–2.00×10^{-4}
ω	2.734×10^{-6}–1.40×10^{-3}
γ	2.34×10^{-6}–2.4×10^{-3}
α_{LZ}	4.16×10^{-4}–8.53×10^{-1}

We sampled an average of 10 000 distinct surface-hopping trajectories each with a time step of $dt = 1.25$ (for select calculations we used more trajectories as detailed in Sec. VI). To determine the transition rate, we plotted the average population on the diabatic surfaces as a function of time. We fit the average diabatic population as a function of time as an exponential rate process to obtain a transition rate. Some of the data showed transient non-exponential behavior at short times, but such phenomena were not significant enough to substantially influence the rates.

In Table I, we provide the relevant parameter ranges as adapted from Hammes-Schiffer[7] (all in atomic units). Results are independent of mass (we chose $m = 1$).

VI. RESULTS AND DISCUSSION

Our first test of the A-FSSH method is recovering the qualitative behavior of the Marcus rates as a function of driving force ϵ_0. We recently found that FSSH recovered the correct behavior,[36] and so A-FSSH should do the same. Indeed, Fig. 3 shows that both FSSH and A-FSSH show standard Marcus behavior, whereby the rate increases with increasing ϵ_0 in the normal Marcus regime, peaking when ϵ_0 is equal to the reorganization energy, and then decreasing with a continued increase in ϵ_0 in the inverted Marcus region. As we would hope, A-FSSH yields a much better approximation to the Marcus rates than does standard FSSH.

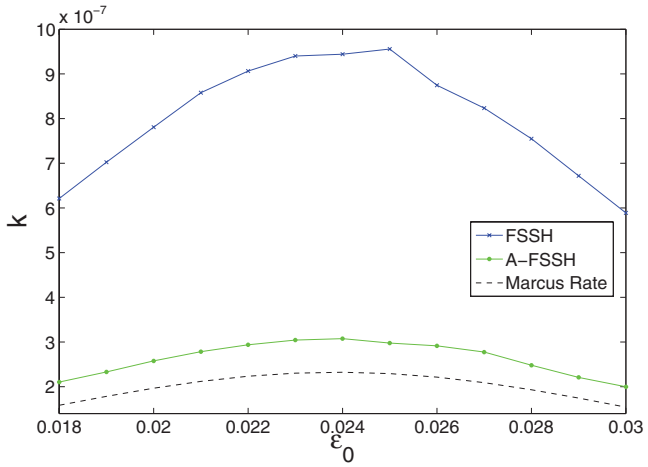

FIG. 3. Comparison of the calculated rates for FSSH and A-FSSH with the expected Marcus rates as a function of ϵ_0 (i.e., the driving force). $E_r = 2.39 \times 10^{-2}$, $\gamma = 1.50 \times 10^{-4}$, $V = 2.50 \times 10^{-5}$, and $\omega = 4.375 \times 10^{-5}$.

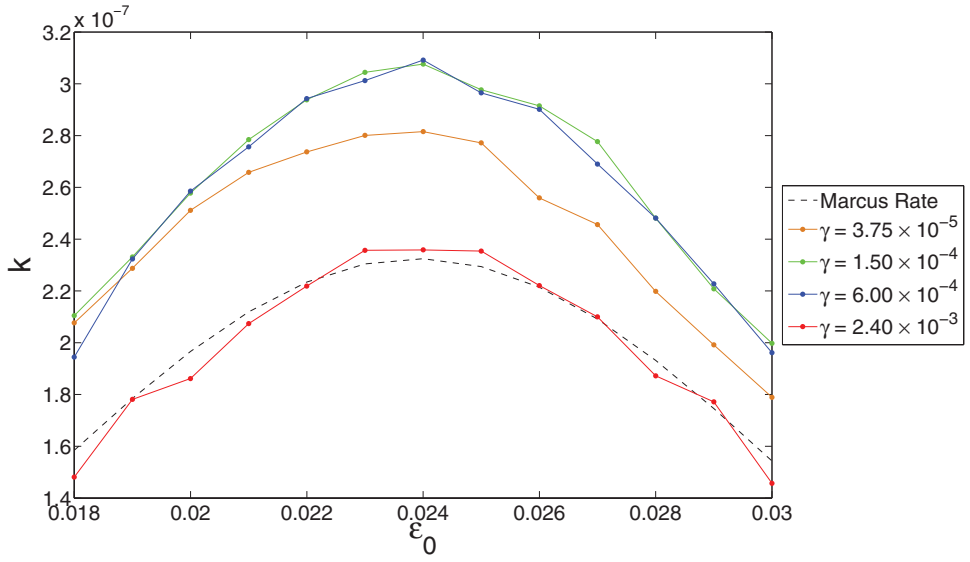

FIG. 4. Comparison of the calculated rates for A-FSSH with the expected Marcus rates as a function of ϵ_0 for a range of values of γ (i.e., the frictional coefficient). $E_r = 2.39 \times 10^{-2}$, $V = 2.50 \times 10^{-5}$, and $\omega = 4.375 \times 10^{-5}$.

Figure 4 shows the A-FSSH rates as a function of ϵ_0 for a range of γ. As expected, the rates increase as γ increases from the underdamped limit to a maximum in the transition state limit, and then decrease again in the overdamped limit. We had found this behavior previously for FSSH (Ref. 36) as well. Kramer's view of frictional effects[49] does hold within our surface-hopping models, predicting a turnover from under to overdamped dynamics. Because the A-FSSH rates only vary by a factor of about 1.5 over the full range of ϵ_0, Fig. 4 required more trajectories to converge the results than other figures. We used 30 000 trajectories for A-FSSH data in Figs. 3 and 4 as compared to 10 000 in the other plots.

In Fig. 5, we show a log-log plot of rate vs. diabatic coupling V. As we found in Ref. 36, FSSH scales linearly with V (incorrectly). By contrast, A-FSSH nearly matches the simple collapse method, which scales quadratically in V (correctly).[36] Intuitively, one might expect that A-FSSH should give even better results than the simple collapse method because A-FSSH allows for decoherence events on both the upper and lower adiabatic surfaces, while simple collapse restricts decoherence events to the lower adiabatic surface (in the normal regime). Physically, the A-FSSH picture is correct since wave packets can separate (or decohere) each and every time the nuclear trajectory passes through a region of derivative coupling (in both directions). In practice, A-FSSH results outperform simple collapse, yielding results that are noticeably closer to the expected Marcus rate over most of the range of V, except for very small V. Apparently, for very small V, the A-FSSH method predicts collapsing events less frequently and merely returns the simple collapse results. Eventually, for truly infinitesimal V in the limit of a conical intersection, A-FSSH might face new problems because of its linear approximation competing with enormous derivative couplings—but we have not experienced such a problem in any of our calculations.

Figure 6 is an important illustration of how the different dynamical regimes are determined by the values of γ and V as discussed in Sec. V B. As V decreases from right to left,

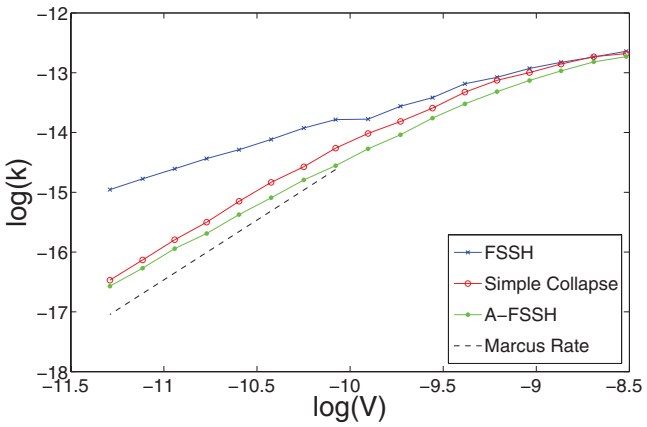

FIG. 5. Log-log plot (base e) comparing the calculated rates for A-FSSH and FSSH with the expected Marcus rates as a function of V (i.e., the diabatic coupling). $\gamma = 1.50 \times 10^{-4}$, $\epsilon_0 = 0.018$, and $\omega = 4.375 \times 10^{-5}$.

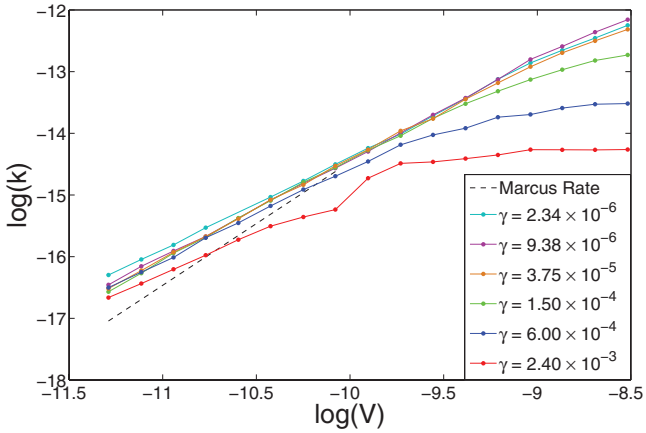

FIG. 6. Log-log plot (base e) comparing the calculated rates for A-FSSH with the expected Marcus rates as a function of V for a range of values of γ. $\epsilon_0 = 0.018$ and $\omega = 4.375 \times 10^{-5}$.

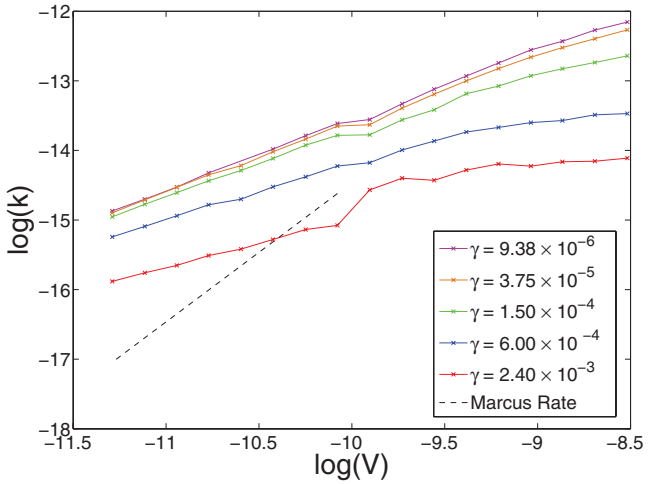

FIG. 7. Log-log plot (base e) comparing the calculated rates for FSSH with the expected Marcus rates as a function of V for a range of values of γ. $\epsilon_0 = 0.018$ and $\omega = 4.375 \times 10^{-5}$.

the Landau-Zener parameter α_{LZ} decreases as well, and the system moves fully into the nonadiabatic regime. Figure 6 shows that it is only in this regime that any of our results agree with the Marcus rates. This behavior is quite natural since Marcus theory is derived from Fermi's golden rule (perturbation theory), and holds only when V is small. (For this reason, we plot the Marcus rates only in the small V regime.) Additionally, Fig. 6 illustrates how γ affects the rates. For the larger values of γ, the system is mostly in the overdamped regime not the transition state regime. We need $\frac{\sqrt{E_r kT}\omega}{V} \gg \gamma$ to be in the transition state regime, but for the largest values of γ this condition holds only on the far left of the plot, where our calculated A-FSSH rate always approaches the Marcus rate. Similarly, when V is large, the very smallest values of γ press up against the other transition state condition, $\gamma \gg \frac{V^2}{\sqrt{E_r kT}}$. This condition affects only the far right side of the plot for the smallest two values of γ. Overall, Fig. 6 suggests that the A-FSSH algorithm captures the correct behavior of the rate as a function of V and γ; by contrast,

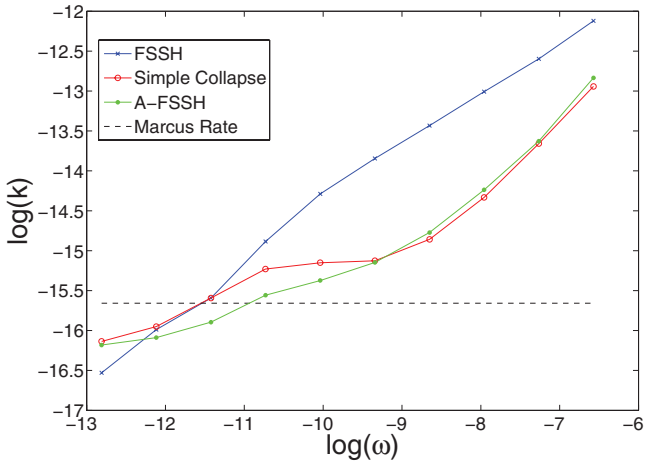

FIG. 8. Log-log plot (base e) comparing the calculated rates for FSSH and A-FSSH with the expected Marcus rates as a function of ω (i.e., the harmonic frequency). $\gamma = 1.50 \times 10^{-4}$, $\epsilon_0 = 0.018$, and $V = 2.50 \times 10^{-5}$.

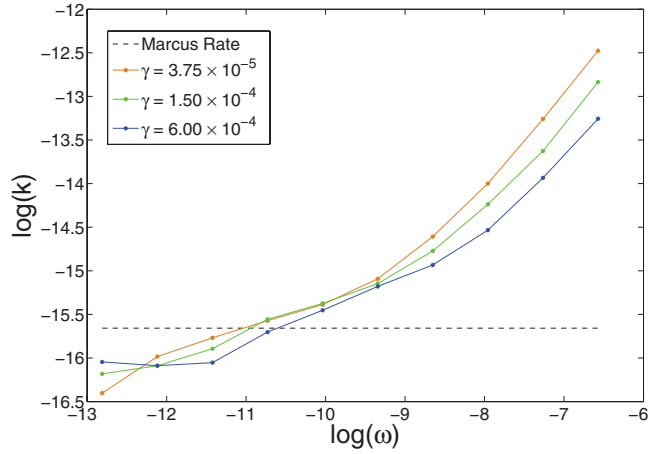

FIG. 9. Log-log plot (base e) comparing the calculated rates for A-FSSH with the expected Marcus rates as a function of ω for a range of values of γ. $\epsilon_0 = 0.018$, and $V = 2.50 \times 10^{-5}$.

FSSH predicts qualitatively different and largely incorrect behavior by failing to include decoherence (see Fig. 7).

One item not addressed in Ref. 36 is the fact that the transition rate was found in that paper to depend on ω, both for FSSH *and* when simple collapses were applied. To further investigate this effect, we plot in Fig. 8 the dependence of the rate on ω. We find that for small enough values of ω, the log-log plots of A-FSSH rates vs. ω flatten out roughly as they should (Fig. 9). We find this behavior only for small ω, which puts us in the high temperature limit of Marcus theory, $\hbar\omega \ll kT$. Notably, even at high temperatures, our A-FSSH results still display some weak and unexplained dependence on ω. By contrast, the standard FSSH rates are strongly dependent on ω over our entire parameter range (Fig. 10).[53]

In summary after gathering a great deal of data, we find that adding decoherence corrects the major shortcomings that plagued the FSSH algorithm in Ref. 36 as applied to the spin-boson model. Additionally, we have shown that A-FSSH, which is generalizable to more complicated systems, has the correct physical behavior for the spin-boson system and agrees with an *ad hoc* simple collapse method based

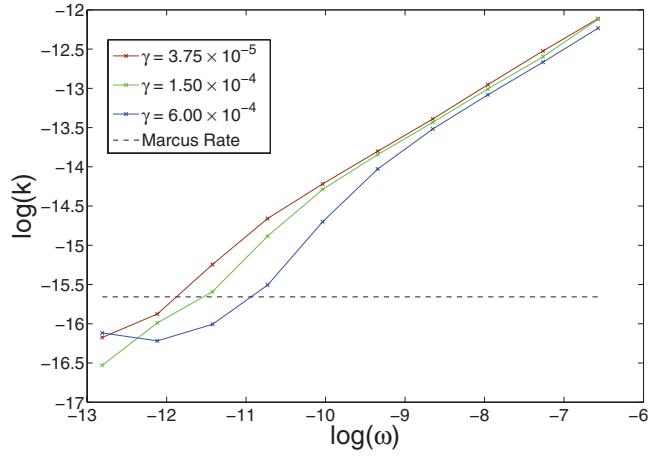

FIG. 10. Log-log plot (base e) comparing the calculated rates for FSSH with the expected Marcus rates as a function of ω for a range of values of γ. $\epsilon_0 = 0.018$ and $V = 2.50 \times 10^{-5}$.

on our intuitive understanding of the physics. Not only is A-FSSH qualitatively correct, but we find it to have a final error in rates of only a factor of about 1.5 when compared with the correct Marcus results.

Finally, with regards to computational efficiency, A-FSSH is computationally slower than FSSH because it propagates the moments as well as the other dynamical variables, but the speed difference is only a factor of about 4. We expect therefore that, for increased accuracy, A-FSSH will be well worth the cost when running future applications to determine rates of relaxation of photo-induced, nonadiabatic processes in the condensed phase.

VII. CONCLUSION

We have shown that A-FSSH correctly produces the correct qualitative Marcus rate behavior for the spin-boson model. It captures the correct scaling with diabatic coupling that standard FSSH is unable to reproduce. It also gives a rate independent of ω for small enough values of ω (i.e., the relatively high temperature limit). Since calculating rates for the spin-boson model in the small diabatic coupling limit is exquisitely sensitive to the degree of decoherence in surface hopping calculations, this model problem has allowed us to fine-tune and simplify the A-FSSH method. Clearly, future developments in the field of surface hopping must be benchmarked against this same model problem; modern approaches to decoherence have rarely been tested against such cases of multiple curve crossings. For our part, we look forward to applying A-FSSH to higher dimensional and more realistic systems, given that the computational cost of the algorithm remains minimal.

ACKNOWLEDGMENTS

We thank S. Hammes-Schiffer, A. Soudackov, M. Ratner, A. Nitzan, and M. Newton for very illuminating and helpful conversations. This work was supported by the (U.S.) Air Force Office of Scientific Research (USAFOSR) (Grant No. FA9550-11-0092).

[1] G. Stock and M. Thoss, Phys. Rev. Lett. **78**, 578–581 (1997).
[2] M. Ben-Nun, J. Quenneville, and T. J. Martnez, J. Phys. Chem. A **104** (22), 5161–5175 (2000).
[3] I. R. Craig and D. E. Manolopoulos, J. Chem. Phys. **121**, 3368–3373 (2004).
[4] W. H. Miller, J. Phys. Chem. A **113**, 1405–1415 (2009).
[5] J. C. Tully, J. Chem. Phys. **93**(2), 1061–1071 (1990).
[6] G. A. Jones, B. K. Carpenter, and M. N. Paddon-Row, J. Am. Chem. Soc. **120**(22), 5499–5508 (1998).
[7] A. Hazra, A. V. Soudackov, and S. Hammes-Schiffer, J. Phys. Chem. B **114**, 12319–12332 (2010).
[8] D. Nachtigallova, A. J. A. Aquino, J. J. Szymczak, M. Barbatti, P. Hobza, and H. Lischka, J. Phys. Chem. A **115**, 5247–5255 (2011).
[9] G. Granucci and M. Persico, J. Chem. Phys. **126**, 134114 (2007).
[10] S. A. Fischer, C. T. Chapman, and X. Li, J. Chem. Phys. **135**, 144102 (2011).
[11] S. Fernandez-Alberti, V. D. Kleiman, S. Tretiak, and A. E. Roitberg, J. Phys. Chem. A **113**, 7535–7542 (2009).
[12] M. S. Topaler, T. C. Allison, D. W. Schwenke, and D. G. Truhlar, J. Phys. Chem. A. **102**(10), 1666–1673 (1998).
[13] M. D. Hack, A. M. Wensmann, D. G. Truhlar, and M. Ben-Nun, and T. J. Martnez, J. Chem. Phys. **115**, 1172–1186 (2001).
[14] U. Müller and G. Stock, J. Chem. Phys. **107**, 6230–5245 (1997).
[15] J. Y. Fang and S. Hammes-Schiffer, J. Phys. Chem. A **103**, 9399–9407 (1999).
[16] J. E. Subotnik and N. Shenvi, J. Chem. Phys. **134**, 024105 (2011).
[17] J. E. Subotnik and N. Shenvi, J. Chem. Phys. **134**, 244114 (2011).
[18] F. Webster, P. J. Rossky, and R. A. Friesner, Comput. Phys. Commun. **63**, 494–522 (1991).
[19] F. Webster, E. T. Wang, P. J. Rossky, and R. A. Friesner, J. Chem. Phys. **100**, 4835–4847 (1994).
[20] B. J. Schwartz, E. R. Bittner, O. V. Prezhdo, and P. J. Rossky, J. Chem. Phys. **104**, 5942–5955 (1996).
[21] K. F. Wong and P. J. Rossky, J. Chem. Phys. **116**, 8418–8428 (2002).
[22] K. F. Wong and P. J. Rossky, J. Chem. Phys. **116**, 8429–8438 (2002).
[23] O. V. Prezhdo and P. J. Rossky, J. Chem. Phys. **107**, 825–834 (1997).
[24] O. V. Prezhdo, J. Chem. Phys. **111**, 8366–8377 (1999).
[25] M. J. Bedard-Hearn, R. E. Larsen, and B. J. Schwartz, J. Chem. Phys. **123**, 234106 (2005).
[26] R. E. Larsen, M. J. Bedard-Hearn, and B. J. Schwartz, J. Phys. Chem. B **110**, 20055–20066 (2006).
[27] C. Zhu, A. W. Jasper, and D. G. Truhlar, J. Chem. Phys. **120**, 5543–5557 (2004).
[28] C. Zhu, S. Nangia, A. W. Jasper, and D. G. Truhlar, J. Chem. Phys. **121**, 7658–7670 (2004).
[29] A. W. Jasper and D. G. Truhlar, J. Chem. Phys. **123**, 064103 (2005).
[30] C. Zhu, A. W. Jasper, and D. G. Truhlar, J. Chem. Theory Comput. **1**, 527–540 (2005).
[31] A. W. Jasper and D. G. Truhlar, J. Chem. Phys. **127**, 194306 (2007).
[32] J. Y. Fang and S. Hammes-Schiffer, J. Chem. Phys. **110**, 11166–11175 (1999).
[33] N. Shenvi, J. E. Subotnik, and W. Yang, J. Chem. Phys. **134**, 144102 (2011).
[34] M. Thachuck, M. Y. Ivanov, and D. M. Wardlaw, J. Chem. Phys. **109**, 5747 (1998).
[35] I. Horenko, C. Salzmann, B. Schmidt, and C. Schutte, J. Chem. Phys. **117**, 11075 (2002).
[36] B. R. Landry and J. E. Subotnik, J. Chem. Phys. **135**, 191102 (2011).
[37] J. E. Subotnik, J. Phys. Chem. A **115**, 12083–12096 (2011).
[38] E. Neria and A. Nitzan, J. Chem. Phys. **99**, 1109 (1993).
[39] A. P. Horsfield, D. R. Bowler, A. J. Fisher, T. N. Todorov, and C. G. J. Sanchez, J. Phys.: Condens. Matter **16**, 8251 (2004).
[40] A. P. Horsfield, D. R. Bowler, A. J. Fisher, T. N. Todorov, and C. G. J. Sanchez, J. Phys.: Condens. Matter **17**, 4793 (2005).
[41] E. J. Heller, J. Chem. Phys. **62**, 1544 (1975).
[42] We found empirically that running A-FSSH trajectories without the reset criterion in Sec. IV A 4 led to collapses occurring with some regularity in the region of derivative coupling. This led to transition rates that were nearly independent of V for smaller values of V. These unphysical results can be explained computationally because collapsing within a derivative coupling region throws away valuable information in the electronic wavefunction, and that information precisely determines whether or not a trajectory will stay on the current surface or hop to another surface as it passes through the coupling region. Wiping out this information within the coupling region must therefore lead to problems. By the time a trajectory has left the coupling region, however, all hops have been completed already, so that the electronic amplitudes have served their purpose and it is acceptable (and often necessary) to collapse the electronic wavevector.
[43] The potential energy surfaces for Fig. 1: $V_{11}(x) = 0.03\tan(1.6x)$, $V_{22}(x) = -0.03\tan(1.6x)$, and $V_{12}(x) = 0.005e^{-x^2}$.
[44] A. J. Leggett, S. Chakravarty, A. T. Dorsey, M. P. A. Fisher, AI Garg, and W. Zwerger, Rev. Mod. Phys. **59**, 1–85 (1987).
[45] D. E. Makarov and N. Makri, Phys. Rev. A **48**, 3626–3635 (1993).
[46] D. Mac Kernan, G. Ciccotti, and R. Kapral, J. Chem. Phys. **116**, 2346–2353 (2002).
[47] M. Ben-Nun and T. J. Martinez, Isr. J. Chem. **47**, 75–88 (2007).
[48] R. A. Marcus, J. Chem. Phys. **24**, 966 (1956).
[49] A. Nitzan, *Chemical Dynamics in Condensed Phases* (Oxford University Press, 2006).
[50] H. A. Kramers, Physica **7**, 284–304 (1940).
[51] J. C. Tully, G. H. Gilmer, and M. Shugard, J. Chem. Phys. **71**(4), 1630–1642 (1979).
[52] D. Beeman, J. Comput. Phys. **20**, 130–139 (1976).
[53] Interestingly, according to Figure 10, at small enough values for γ, standard FSSH gives a rate independent of ω, though we do not find any physical meaning behind this behavior.